Catalysis Science & Technology

ROYAL SOCIETY OF CHEMISTRY

PAPER

View Article Online
View Journal | View Issue



Cite this: *Catal. Sci. Technol.*, 2024, **14**, 3514

# Monitoring the influence of steam on highly-active rhodium catalyst during the combined reforming of biogas by transient and steady-state *operando* spectroscopic studies

Victoria Garcilaso, Rubén Blay-Roger, Miriam González-Castaño, Luis F. Bobadilla, Miguel A. Centeno and José A. Odriozola *

Received 20th February 2024,
Accepted 6th May 2024

DOI: 10.1039/d4cy00236a

rsc.li/catalysis

The impact derived from incorporating water into $CH_4/CO_2$ biogas stream for the generation of syngas was investigated over the $Rh/MgAl_2O_4$ catalyst using *operando* steady-state and transient DRIFT spectroscopy coupled with MS. The incorporation of steam resulted in improved $CH_4$ conversion rates and attained syngas streams with higher $H_2/CO$ ratios. It was demonstrated that in the presence of steam, the generation of $CH_xO$ species through the reaction of CO* with active *OH species is favored at the metal support surface. Besides, the enhanced resistance delivered by water molecules towards deactivating the coking phenomena was associated with easier carbonaceous decomposition and the exposition of the very active Rh (100) surfaces for methane decomposition. The $Rh/MgAl_2O_4$ catalyst was demonstrated to be an effective catalyst for the production of $H_2$-rich syngas streams. More importantly, the insights reported herein provide new evidences regarding the impact of steam on biogas reforming reactions.



## 1. Introduction

Over the last several years, the production of biogas from the anaerobic digestion of biomass wastes has attracted considerable interest as a renewable carbon source.[1,2] As biogas is composed mainly of $CH_4$ and $CO_2$, the production of syngas by the reforming of biogas and the subsequent transformation into liquid fuels *via* Fischer–Tropsch synthesis (FTS) is the most suitable process and the most cost-effective from the industrial point of view.[3,4] However, the chemical composition of raw biogas depends on the type of feedstock, design of the digester-fermenter and operating conditions.[5–7] Typically, biogas contains 60–75 vol% of methane and 19–33 vol% of $CO_2$ along with moisture besides other contaminants such as sulphur compounds, halogenated compounds, ammonia, organic silicon compounds (siloxanes), tars, and particulate matter.[8–10] The most usual technologies applied to remove contaminants from raw biogas during the upgradation process include membrane technology, water scrubbing, pressure swing adsorption (PSA), cryogenic separation and biological techniques.[11]

Apparently, the presence of steam in biogas is not a drawback but a major advantage for reforming processes.[12] Although the formation of carbon is thermodynamically limited at typical reforming temperatures, the deposition of coke on the catalyst surface is unavoidable in the dry reforming reaction of methane.[13] The formation of carbon can be minimized due to the presence of steam, which provides a higher oxidant level throughout the carbon gasification reaction. Unlike the dry reforming of model biogas, in which the syngas obtained is always present at a $H_2/CO$ ratio lower than one, the presence of water produces a syngas more flexible by adjusting the $CO_2/H_2O$ ratio to match the desired value close to 2 required for the downstream production of the chemical value-added *via* Fischer–Tropsch synthesis.[14] In this scenario, the combination of dry reforming of methane (DRM) and steam reforming of methane (SRM) has been explored extensively and it is known as the bi-reforming of methane[15] or also the combined reforming of methane.[16] This approach has attracted great interest from the industrial point of view and provides an opportunity for advanced research toward the commercialization of this technology.[17,18]

Catalysts used for combined reforming processes are usually based on nickel, but their stability is limited by the metal sintering and/or coke deposition processes.[19,20] Stroud *et al.*[21] proposed an Sn–Ni/Ce–Al catalyst able to enhance both methane conversion and catalytic stability in the presence of steam in the bi-reforming of methane compared to the same catalyst tested under dry-reforming conditions. On the other hand, MgO and $Al_2O_3$ have been probed as the most promising

*Departamento de Química Inorgánica and Instituto de Ciencia de Materiales de Sevilla, Centro Mixto Universidad de Sevilla – CSIC, Av. Américo Vespucio 49, 41092 Sevilla, Spain. E-mail: odrio@us.es*

supports for the dry reforming of methane. It is well known that the increased basicity of the support favours the adsorption of $CO_2$, facilitating the gasification of carbon to form CO, as Zhao *et al.*[22] reported in a recent study. Herein, a bimetallic Ni–Co/$MgAl_2O_4$ catalyst showed a high stability over more than 30 h under reforming atmospheres without evidence of carbon deposits in the presence of $H_2O$ and $CO_2$. In a microkinetic study, Geng *et al.*[23] argued that oxygen atoms from steam promoted methane conversion by switching the reaction path from $CH_3^* + * \rightarrow CH_2^* + H^*$ to $CH_3^* + O^* \rightarrow CH_2^* + OH^*$ whilst restricting the generation of C* species, which constricted the generation of carbon deposits. With most of the studies focusing on Ni catalysts, the incorporation of adequate steam concentrations could increase the $H_2:CO$ ratios and improve the catalyst stability by favouring the gasification of carbon deposits.[24] In this sense, the larger OH concentrations over Ni catalysts generated in the presence of steam were proposed to enhance the gasification of carbon deposits generating CHO* species.[25] Still, deactivation issues related to metal sintering and the partial oxidation of the active sites have also been reported.[26,27]

Although their limited availability and high cost restrain their use for large-scale applications, noble metals like Pt, Ru, Pd and Rh attain higher conversions and major coke resistance than transition metals.[13] Among them, Rh was demonstrated to be the most active towards the conversion of methane when supported on $CeO_2/Al_2O_3$.[13] Over different supports and reaction conditions, Rh metal also exhibited the highest turnover frequency (TOF) compared to their homologues based on Ru and Pt.[28] Maestri *et al.*[29] proposed a consistent microkinetic model on Rh catalyst that pointed out the mechanistic analogies between steam and dry reforming. They proposed that methane consumption proceeds *via* decomposition and subsequent carbon oxidation by OH* following a sequential route ($CH_4 \rightarrow C^* \rightarrow CO^*$), and the role of either $CO_2$ or $H_2O$ is to provide the main oxidizer (OH*). Rostrup-Nielsen and Bak Hansen[30] also observed that replacing steam by carbon dioxide hardly modified the reforming mechanism. Moreover, they demonstrated that Ru and Rh catalysts are highly stable for carbon-free operation, presenting high reforming rates combined with low coke formation rates.

*Operando* diffuse reflectance infrared Fourier transform spectroscopy (DRIFTS) has been widely employed as a powerful tool to elucidate the reaction mechanism and gain insights into the nature of surface intermediates. In a previous work,[31] we studied the activity of the Rh/$MgAl_2O_4$ catalyst toward the biogas reforming reaction using transient and steady-state DRIFTS experiments, proposing a reaction mechanism in which the dissociative adsorption of $CO_2$ takes place initially and the active oxygen species formed on the metallic sites facilitates C–H bond activation. Although numerous articles have been published on the dry reforming of methane reaction on different supported Rh catalysts, there is not a clear and unambiguous explanation of the real effect of steam on the nature of the reaction. The scarce studies focusing on the role of steam and OH surface groups on the reaction mechanism and constituted intermediates might be associated with the low concentration established under DRM atmospheres.[32] Considering the impact of larger OH coverages generated in the presence of steam and the structure sensitivity character of reforming processes,[33,34] establishing the role of steam for catalytic systems aside of Ni metal is extremely convenient. The present study contributes a new perspective to understand the effect of steam in the activation process of $CO_2$ and $CH_4$ during the reforming of biogas by means of transient experiments and DRIFTS coupled MS studies over the Rh/$MgAl_2O_4$ catalyst. The integration of both transient and steady-state *operando* experiments provides a comprehensive vision of the catalyst surface properties, and their correlation with catalytic performance is very useful for achieving the rational design of catalysts.

## 2. Experimental details

A catalyst based on 1 wt% of Rh dispersed on $MgAl_2O_4$ support was used in this study. The preparation method and characterization details of this catalyst have been described in a previous work.[31] This catalyst was labelled as Rh/$MgAl_2O_4$.

The biogas reforming reaction was carried out in a commercial computerized microactivity reference catalytic reactor from PID Eng & Tech employing a stainless-steel reactor with 9 mm internal diameter. A fixed-bed composed by 50 mg of catalyst diluted in SiC (both sieved in 100–200 μm) to ensure a good heat and mass transfer was placed at the centre of the reactor in direct contact with a thermocouple. Before catalyst testing, the sample was *in situ* reduced in a flow of 50% $H_2/N_2$ at 750 °C for 3 h (100 mL $min^{-1}$). Then, 50 mL $min^{-1}$ of nitrogen was used to purge the reactor system for 30 min before reaction experiments at 750 °C. The reaction was performed at 750 °C and 1 bar, maintaining a total flow rate of 100 mL $min^{-1}$ with a weight hourly space velocity (WHSV) equal to 200 L $h^{-1}$ $g^{-1}$ and varying amounts of steam. Reactant gas mixtures consisting of $CH_4$, $CO_2$, and $N_2$ with a $CH_4/CO_2$ molar ratio equal to 1.5 were introduced using mass-flow controllers from Bronkhorst. Variable amounts of $H_2O$ were introduced using a HPLC pump (Gilbson Inc series) and evaporated to reach concentrations of 8, 12 and 17 vol% of steam. In order to maintain the space velocity and the partial pressures of $CO_2$ and $CH_4$, the flow of nitrogen was adjusted as a function of the steam incorporated. The reforming tests were performed under isothermal conditions, and every concentration of steam was maintained for 2 h to guarantee steady-state conditions. The effluent gases were analysed on-line using a micro-gas chromatograph (Varian 4900 model) equipped with two columns: Poraplot Q and molecular sieve 5A. The conversions of methane and $CO_2$ were calculated on the basis of the difference between the input and output of methane and $CO_2$, respectively.

*Operando* DRIFTS-MS experiments were performed in a high temperature reaction chamber (Praying Mantis from Harrick) fitted with ZnSe windows and connected to a Thermo Nicolet Nexus FTIR spectrometer equipped with a liquid $N_2$-cooled MCT detector. Spectra were obtained with a spectral resolution of 4 $cm^{-1}$ and an average of 128 scans. The whole optical path

was continuously purged with a flow of water vapour- and $CO_2$-free nitrogen, and the background spectrum was collected using an aluminium reflective mirror. Typically, about 80 mg of sample was put in the DRIFTS cell to ensure that the gases pass through the catalyst packed-bed mimicking the plug-flow condition of the reaction. Prior to the measurements, the sample was activated *in situ* at 750 °C for 1 h in 50% $H_2$/Ar at a total flow rate of 50 mL $min^{-1}$ and then cooled down to the reaction temperature by purging with Ar. The spectrum of the activated catalyst was used as the reference. The dry biogas reforming reaction was performed by feeding into the cell a gas mixture of 10 vol% $CO_2$ and 15 vol% $CH_4$ balanced in argon with a total flow rate of 50 mL $min^{-1}$. Analogously, the bi-reforming reaction of biogas was carried out using a mixture of 10 vol% of CO, 15 vol% $CH_4$ and 10 vol% of $H_2O$ in argon with a total flow rate of 50 mL $min^{-1}$. For it, an adequate amount of liquid water was fed continuously using a HPLC pump and vaporising the liquid in a homemade evaporator. In both the reactions, the temperature was increased from 550 °C to 750 °C with intervals of 50 °C, and each temperature was maintained for 30 min to achieve steady-state conditions. For the transient experiments, the feed composition was temporarily varied following two different sequences: 1) 10%$CO_2$/Ar → Ar → 15%$CH_4$/Ar, and 2) 10%$CO_2$/10%$H_2O$/Ar → 10%$H_2O$/Ar → 15%$CH_4$/10%$H_2O$/Ar. The different mixtures were introduced under isothermal conditions at 550 °C every 20 min. A four-way valve was installed to switch the gas mixtures. The gas composition exiting the DRIFTS cell were sent to a mass spectrometer (PFEIFFER MS Vacuum Prisma Plus) using a 1/16-inch stainless steel capillary tubing heated at 150 °C for analysis to avoid condensation. The continuous data acquisition of MS was recorded using the Quadera software, following mainly the signals $m/z$ = 2, 15, 18, 28 and 44.

## 3. Results and discussion

### 3.1. Effect of steam in the biogas reforming reaction

The effect of different steam concentrations in the biogas reforming reaction over Rh/$MgAl_2O_4$ catalyst was performed under isothermal conditions at 750 °C, feeding a $CH_4$/$CO_2$ molar ratio of 1.5. Fig. 1a shows that the presence of steam promotes the methane conversion but has a contrary effect on $CO_2$ conversion. The general reaction of bi-reforming of methane can be represented by a combination of the steam reforming and dry reforming reactions, as shown in the following equations.

$$\text{Dry reforming of methane: } CH_4 + CO_2 \rightarrow 2CO + 2H_2 \quad (1)$$

$$\text{Steam reforming of methane: } CH_4 + 2H_2O \rightarrow CO + 3H_2 \quad (2)$$

$$\text{Bi-reforming of methane: } 3CH_4 + CO_2 + 2H_2O \rightarrow 4CO + 8H_2 \quad (3)$$

Additionally, a variety of different parallel reactions also can occur, including the following.[35]

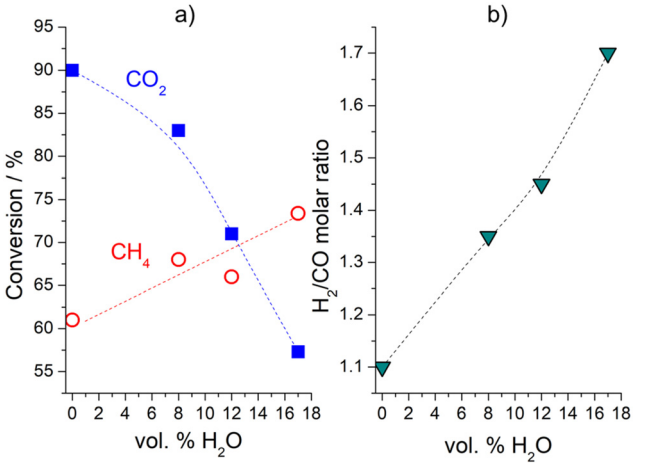


Fig. 1 Effect of the steam concentration on the performance of Rh/$MgAl_2O_4$ in terms of a) $CO_2$ and $CH_4$ conversion, and b) $H_2$/CO molar ratio during the biogas reforming reaction tested under WHSV = 200 L $h^{-1}$ $g^{-1}$, $T$ = 750 °C and $CH_4$/$CO_2$ molar ratio = 1.5.

$$\text{Water gas shift reaction (WGS): } CO + H_2O \leftrightarrow CO_2 + H_2 \quad (4)$$

$$\text{Methane decomposition: } CH_4 \leftrightarrow C + 2H_2 \quad (5)$$

$$\text{Boudouard reaction: } CO_2 + C \leftrightarrow 2CO \quad (6)$$

$$\text{Beggs reaction: } C + H_2O \leftrightarrow H_2 + CO \quad (7)$$

$$\text{CO}_2\text{ methanation: } CO_2 + 4H_2 \rightarrow CH_4 + 2H_2O \quad (8)$$

$$\text{CO methanation: } CO + 3H_2 \rightarrow CH_4 + H_2O \quad (9)$$

The enhancement of the $CH_4$ conversion with the amount of water in the feed is mainly due to the participation of the steam reforming reaction (eqn (2)), whereas the lower $CO_2$ conversion is related to the $CO_2$ produced by the WGS reaction (eqn (4)). An increase in the concentration of water favours the WGS reaction against the dry reforming of methane, resulting in a negative $CO_2$ balance, as predicted the by thermodynamics.[15,21]

Furthermore, Fig. 1b shows that the $H_2$/CO molar ratio increases from 1.1 to 1.7 by increasing the vol% of water, which is strictly related to the production of hydrogen and the consumption of CO by the WGS reaction and the gasification of carbonaceous deposits (eqn (7)). In a collaboration work of our group, Stroud *et al.*[21] reported a similar $H_2$/CO ratio of 1.6 for a feed of $CH_4$/$CO_2$/$H_2O$ = 1/1/1 (33 vol% of $H_2O$) at 700 °C on a bimetallic Ni–Sn supported catalyst. Moreover, it was demonstrated that the introduction of water in the bi-reforming reaction favours the gasification of carbonaceous species deposited on the catalyst surface. Roh *et al.*[36] found an optimal $CO_2$ : $H_2O$ : $CH_4$ feed ratio to obtain the syngas with a $H_2$/CO molar ratio of 2 suitable for Fischer–Tropsch synthesis. The optimal concentration of water reported by these authors was 25 vol% of steam for a $CH_4$/$CO_2$ ratio of 2.5. In another previous work, we found

 

that an $H_2/CO$ ratio close to 2 can be achieved using a feed of 28 vol% of water and a $CH_4/CO_2$ ratio of 2.5 over a Ni–Ru-based catalyst. In the current work, the reaction was performed using a typical biogas composition with a $CH_4/CO_2$ ratio of 1.5 and concentrations of water below 20 vol%. Nevertheless, the tendency observed for the $H_2/CO$ ratio with the water concentration (Fig. 1b) suggests that water concentration of about 8 to 18 vol% should result in industrially relevant $H_2/CO$ molar ratios.

### 3.2. *Operando* DRIFTS-MS studies

*Operando* DRIFTS-MS studies were performed to better understand the influence of steam and the intermediate species formed during the dry reforming and bi-reforming of biogas reaction over $Rh/MgAl_2O_4$ catalyst. A comprehensive vision of the reaction mechanism provides a useful guidance to design an optimal catalyst in terms of the activity, selectivity, and stability.

**3.2.1. *In situ* reduction pretreatment.** The sample was reduced in 50%$H_2$/Ar at 750 °C for 1 h to clean the catalyst surface, ensuring the complete reduction of Rh particles. Fig. 2 gives an account of the evolution of the DRIFT spectra during the activation treatment as a function of the temperature. In the initial stage at RT, the fresh sample presents a characteristic band at 1647 $cm^{-1}$ assigned to the deformation mode of adsorbed water on the surface[37] and several bands in the 1600–1300 $cm^{-1}$ spectral region that can be attributed to residual carbonate-like species formed by the interaction with the atmospheric $CO_2$ of the hydroxylated $MgAl_2O_4$ surface.[38]

Heating up the sample in the reduction flow, the physisorbed water disappeared completely at temperatures near 140 °C and on increasing the temperature above 450 °C, one band at 3720 $cm^{-1}$ appeared, which is ascribable to "free" hydroxyls, disclosing the complete dehydration of the surface by the elimination of the broad band centred at *ca.* 3500 $cm^{-1}$ associated with the H-bonded hydroxyls of weakly adsorbed water.[39] The evolution of the bands assigned to carbonate species during the pretreatment suggests the different thermal stability and reactivity towards hydrogen. It is noteworthy that as the temperature increases above 200 °C, an alteration of the carbonate features is observed, and new bands appeared at 2010 and 1915 $cm^{-1}$, which can be assigned to Rh-carbonyl species with different coordination geometries, respectively.[40] It is well known that the thermal decomposition and/or reduction of carbonate species takes place in the presence of hydrogen over noble metals, leading to the formation of Rh-carbonyl intermediate species and CO gas at temperatures of 200–300 °C.[41] Because Rh is an optimal active metal for the methanation reaction, the dissociation of CO on Rh particles to form "C" species and their subsequent hydrogenation to form methane gas should not be ruled out.[42] In this sense, the disappearance of Rh-carbonyl species as the temperature is increased above 300 °C suggests the possible methanation of adsorbed CO. Nevertheless, the low concentration of methane formed is too low to be detected using an IR spectrometer. When the temperature reached 750 °C, all carbonate species were removed, indicating that the pretreatment is effective to obtain a clean surface. We can conclude that apparently the catalyst surface only contains "free" hydroxyls and Rh metallic particles highly dispersed after reduction pretreatment for 1 h at 750 °C.

**3.2.2. Steady-state dry and bi-reforming of biogas.** The influence of steam was investigated by *operando* DRIFTS-MS on the Rh-based catalyst under reaction conditions. For this purpose, 10 vol% steam was selected and compared with the

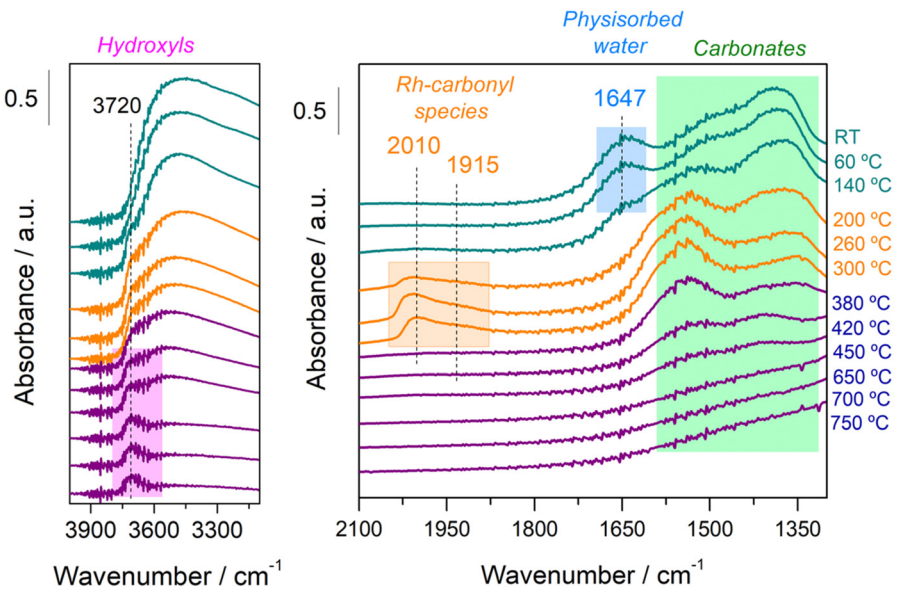


Fig. 2 Evolution of the DRIFT spectra with the temperature in the 4000–3100 and 2100–1300 $cm^{-1}$ regions during the reduction pretreatment at 750 °C for 1 h in 50%$H_2$/Ar over the Rh catalyst.

dry conditions. Fig. 3 shows the evolution of the DRIFT spectra with temperature in the absence (Fig. 3a) and presence (Fig. 3b) of water in the reaction mixture.

As shown Fig. 3a, after introducing the reacting gas mixture of $CO_2$ and $CH_4$ free of water at 550 °C, a prominent peak at 2360 $cm^{-1}$ associated with the asymmetric stretching ($\nu_{as}$) of $CO_2$ gas and two bands at 3016 and 1303 $cm^{-1}$ associated with the rotational fine structure of methane gas appear.[43] The bands appearing at 2030–2008 $cm^{-1}$ and 1920–1860 $cm^{-1}$ indicate the formation of linearly adsorbed CO and bridged CO species on Rh sites, suggesting that $CO_2$ is dissociated into CO and "O" species.[40] With increasing temperature, the appearance of the characteristic *P* branch between 2140 and 2200 $cm^{-1}$ of the gaseous CO vibrational-rotational spectrum is more appreciable, which indicates the release of CO gas.[43] Additionally, two complex pair of bands centred at 1595 and 1360 $cm^{-1}$ were identified at lower temperatures. As the temperature increases, these two bands evolve together, giving a set of bands at 1630, 1535, 1377 and 1330 $cm^{-1}$ at 750 °C. These latter bands are associated with the presence of residual carbonaceous species adsorbed on the support surface.[44,45] Regarding the assignment of the bands at 1595 and 1360 $cm^{-1}$, some authors have assigned the band at 1595 $cm^{-1}$ to the $\nu_{as}$(OCO) vibrational mode of the formate species. Nevertheless, the two characteristic bands of the formate species at 1395 and 1375 $cm^{-1}$ ascribed to CH deformation and $\nu_s$(OCO), respectively, were absent in our experimental data (Fig. 3). Additionally, a band at 2900–2800 $cm^{-1}$ ascribed to the $\nu$(C–H) stretching of formate should appear in the spectra. Although this region is overlapped with the rotational fine structure of gaseous methane, the band related to the C–H stretching of formate is hardly observable. Therefore, we cannot attribute these bands to formate species. It is more reasonable to assume that the bands at 1595–1360 $cm^{-1}$ are attributable to monodentate carbonates with $\Delta\nu_3$ of 100–200 $cm^{-1}$ formed on the support's basic sites.[46,47] These species are thermally labile carbonates, which are decomposed or reduced as the temperature increases.

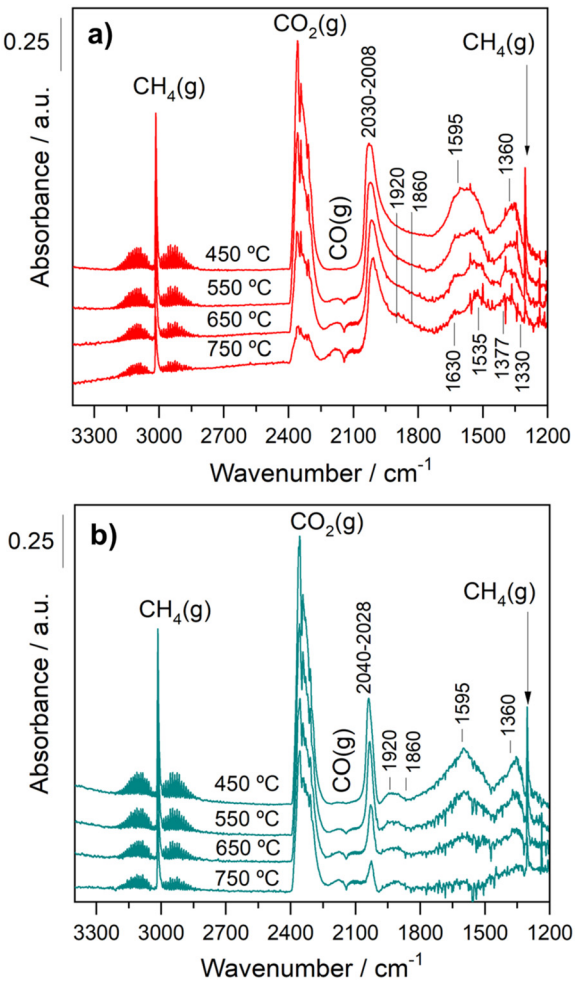


**Fig. 3** Evolution of DRIFT spectra under the reaction conditions as a function of temperature on the reduced sample. Spectra were recorded in the reaction mixture with $CH_4/CO_2$ = 1.5 in the absence of water (a) and the presence of 10 vol% of water (b).

In the presence of water (Fig. 3b), the bands associated with gaseous $CO_2$ and $CH_4$ were also observed, although important differences were noticed in the adsorbed species. In the 1700–1200 $cm^{-1}$ spectral region, it is worth noticing that the bands at 1595 and 1360 $cm^{-1}$ vanished rapidly with the temperature, whereas the bands at 1630, 1535, 1377 and 1330 $cm^{-1}$ were hardly observed. This clearly reveals that steam favours the gasification/decomposition of carbonaceous species. On the other hand, the presence of CO carbonyl adsorbed species over $Rh^0$ sites characterized by the bands at 2040–2028 $cm^{-1}$ and 1920–1860 $cm^{-1}$, assigned to CO adsorbed linearly and multi-bonded carbonyl species, respectively, was also observed.[40,48] Thus, $CO_2$ dissociation also takes place under bi-reforming conditions. Nevertheless, the infrared spectra associated with the carbonyl species were clearly affected by the reaction atmosphere.

The differences in the adsorbed CO species can provide information about the species and sites responsible for the activation of $CO_2$ and $CH_4$ in the presence and absence of steam. In order to assess the influence of the steam on the CO adsorbed species on Rh in detail, Fig. 4 focuses on the different evolutions noticed on increasing the reaction temperature for the 2100–1800 $cm^{-1}$ region. It can be noticed that the increase in the temperature from 450 °C to 750 °C caused a slight decrease in the intensity of the CO adsorption peaks associated with linearly adsorbed CO with a displacement to lower wavenumbers from 2030 to 2008 $cm^{-1}$ in the absence of water (Fig. 4a), while in presence of steam, the equivalent bands were progressively removed with the temperature and displaced from 2048 to 2028 $cm^{-1}$ (Fig. 4b). The vibrational frequency depends on the CO coverage, and the higher frequency observed at high CO coverages is due to the dipole–dipole coupling between the CO adsorbed molecules on neighbouring sites. In the presence of steam, dipole–dipole coupling accounts for the redshift observed for the carbonyl bands due to the lower CO coverage on Rh particles when the temperature is increased. Nevertheless,

 

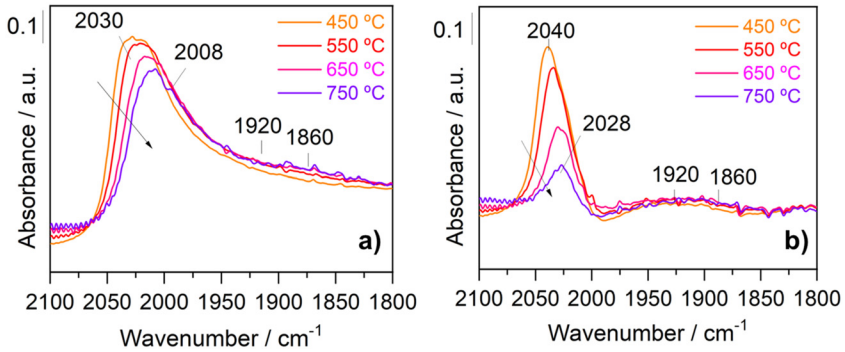


**Fig. 4** Evolution of the DRIFT spectra in the 2100–1800 $cm^{-1}$ region with the temperature for the reduced sample under the reaction conditions in the absence of water (a) and presence of water (b).

the displacement of carbonyl frequencies observed under dry conditions (Fig. 4a) cannot be related to dipole–dipole coupling and CO coverage phenomena. Simultaneously, the band at 2030 $cm^{-1}$ shifts to 2008 $cm^{-1}$ and preserves its intensity, meaning that the electronic density on the rhodium sites increases under these conditions. Accordingly, the formation of carbon species on the surface must be expected, suggesting that CO adsorbs on Rh sites close to carbonaceous deposits that increase the back-donation on the metal surface.[38,49–51] This observation is coherent considering that the absence of water led to the covering of Rh particles by carbonaceous deposits, whereas the water participates in the carbon gasification, cleaning the Rh surface sites. On the other side, it is also noticed from Fig. 5a and b that no shift of the bands attributed to bridge-bonded CO on Rh (1860 and 1920 $cm^{-1}$) was observed with the increase in the reaction temperature. The band at 1860 $cm^{-1}$ has been ascribed to 1 : 2 CO–Rh species while the peak at 1920 $cm^{-1}$ is related to a 3 : 2 stoichiometry.[52] These stoichiometries depend on the type of the rhodium environment and clearly reveal that the presence of steam is affecting the coordination of Rh sites. According to Lavalley *et al.*,[53] these two bands are certainly related to CO adsorption on two rhodium faces such as Rh (100) and Rh (111). The minor presence of the band at 1920 $cm^{-1}$ under dry conditions may be tentatively explained by the blocking of bridged adsorption sites on the corresponding rhodium face. Wang *et al.*[54] studied $CH_4$ dehydrogenation on Rh (111), Rh (110) and Rh (100) surfaces using density functional theory (DFT) calculations. They found that $CH_4$ dehydrogenation on the Rh (100) surface is more favourable in comparison with that on Rh (111) and Rh (110) surfaces. On this basis, carbonaceous deposits formed in the absence of steam could preferentially suppress CO-bridged adsorption on Rh (100) surface sites.

Regarding the evolution of the gas-phase analysed on-line by MS in the absence and presence of steam (Fig. 5a and b), substantial formation of $H_2$ and CO was observed at temperatures above 450 °C during the dry reforming and the bi-reforming of biogas reaction on the Rh catalyst. As the temperature increased, the conversion of methane is higher and the signal of $H_2$ ($m/z$ = 2) is increased. In the absence of

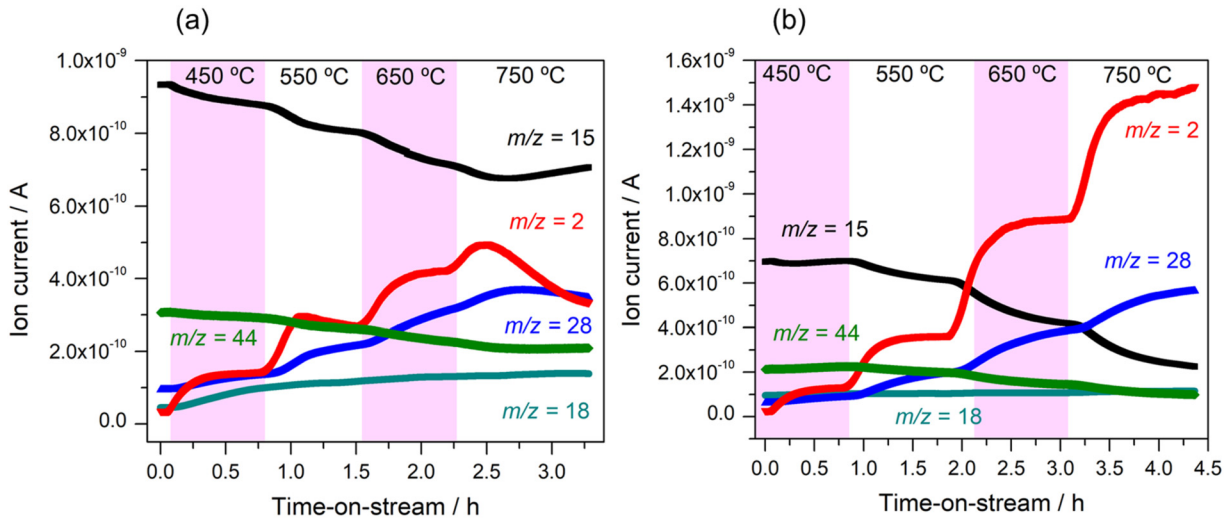


**Fig. 5** Evolution of the gas-phase analysed on-line by MS as a function of time-on-stream and temperature in the absence (a) and presence (b) of steam: $m/z$ = 2 ($H_2$), $m/z$ = 15 ($CH_4$), $m/z$ = 18 ($H_2O$), $m/z$ = 28 (CO) and $m/z$ = 44 ($CO_2$).

water at 750 °C, the significant decrease of methane conversion and $H_2$ concentration was associated with catalyst deactivation due to the formation of carbon deposits or CO species strongly bonded to Rh particles. In agreement with the catalytic activity results, operating in the presence of water resulted in higher $H_2$ concentration and $H_2$/CO ratios close to 2. Remarkably, no signs of catalyst deactivation were noticed in the presence of water, and fairly stable hydrogen production for the entire temperature window was obtained.

**3.2.3. DRIFTS-MS transient studies.** The kinetic responses of the surface species analysed under transient conditions are different from those measured from steady-state experiments and provide direct information about the nature and coverage of surface intermediates. The transient experiments were carried out using different combinations of reactants to analyse the effect of steam. Firstly, we examined the $CO_2$ activation from gas streams containing 10%$CO_2$/Ar, and then we monitored the evolution of the intermediates formed on purging with Ar and subsequently by switching a gas stream containing 15%$CH_4$/Ar. In order to study the impact of steam, we performed an analogous experiment in which the feed composition was temporarily varied following the sequence 1) 10%$CO_2$/10%$H_2O$/Ar → 2) 10%$H_2O$/Ar → 3) 15%$CH_4$/10%$H_2O$/Ar. In both studies, each stream mixture was maintained for 20 min under isothermal conditions at 550 °C.

Fig. 6a and b display the evolution of the IR spectra sequentially recorded by switching the three stream effluents every 20 min in dry and wet conditions, respectively. As can be noticed, under $CO_2$ stream, similar features related to carbonyl adsorbed species and carbonates were observed independently of the presence of water. The presence of both linear (2020–2000 $cm^{-1}$) and bridged (1920–1860 $cm^{-1}$)

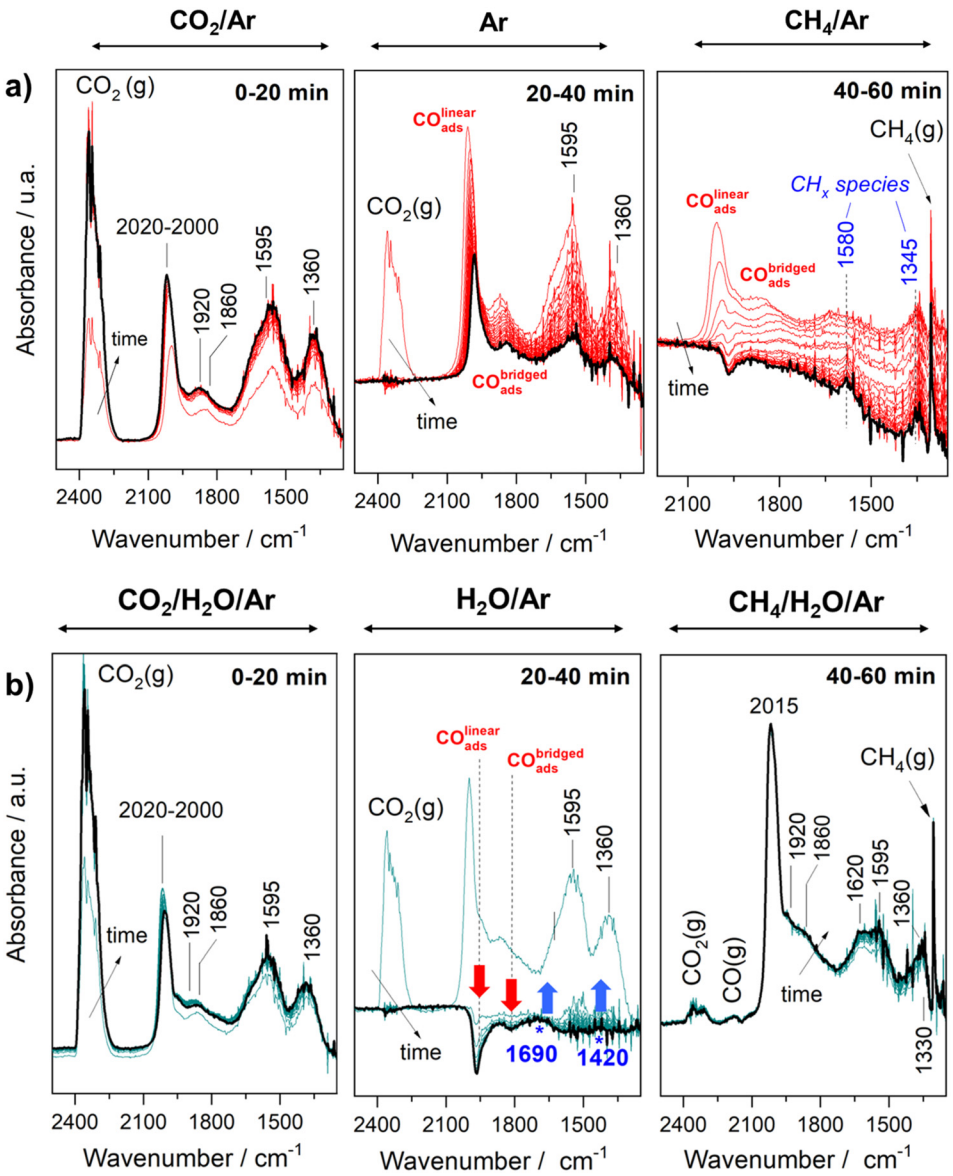


Fig. 6 Evolution of the transient DRIFT spectra observed at 550 °C under the sequential switching of the feed gas in the absence and presence of steam: a) 10%$CO_2$/Ar → Ar → 15%$CH_4$/Ar, and b) 10%$CO_2$/10%$H_2O$/Ar → 10%$H_2O$/Ar → 15%$CH_4$/10%$H_2O$/Ar.

 

carbonyls under both stream conditions indicates that $CO_2$ is dissociated on the metallic sites and that water plays no a significant role in the direct dissociation of $CO_2$. Upon switching the $CO_2$ stream to a purge stream, significant differences were observed in the absence and presence of water. As shown in Fig. 6a, the IR bands attributed to the carbonate species disappeared almost completely, whereas the intensities of the bands attributed to the adsorbed carbonyl species decreased only partially during the Ar purging step. Meanwhile, Fig. 6b reveals that in the presence of steam, the metallic carbonyls and carbonates disappeared very fast. Moreover, it is remarkable to notice the negative evolution of carbonyls and the simultaneous emergence of two bands at 1690 and 1420 $cm^{-1}$. These two bands are assigned to CO stretching and CH bending in the $CH_xO$ species.[55–57] These findings clearly reveal that $CH_xO$ species are reaction intermediates favored in the presence of steam. We can assume that the generation of $CH_xO$ species occurs through the reaction of CO* with the active *OH species formed likely at the metal support interface. Subsequently, by switching the gas feed from purge to $CH_4$ stream, the impact of steam is even more evident. From Fig. 6a, it is evident that the bands related to carbonyls and carbonates completely disappear whereas residual bands at 1580 and 1345 $cm^{-1}$ are developed. These features are ascribed to carbonaceous species.[58,59] The observed negative band of carbonyl could be related to the transformation of linearly adsorbed CO species into –COH adsorbed species. Therefore, these observations clearly reveal that the catalyst's surface is a covering of accumulated carbon formed by methane dissociation in the absence of steam. In contrast, one can see in Fig. 6b that with the incorporation of $CH_4/H_2O$/Ar steam, $CO_2$ and CO gases were released. Furthermore, bands ascribed to carbonyl species adsorbed over Rh metal sites and bands at 1620, 1595, 1360 and 1330 $cm^{-1}$ ascribed to carbonates with different coordination geometry were also detected. The formation of CO and $CO_2$ indicate that gasification and WGS reactions are happening on the catalyst surface.

Finally, Fig. 7a and b display the evolution of gaseous products monitored by on-line mass spectrometry (MS). Ion currents were measured for the *m*/*z* values of the $H_2O$, $CO_2$ $CH_4$, $H_2$ and CO and $H_2O$. Firstly, it must be noticed that a large amount and stable production of hydrogen is achieved in the $CH_4/H_2O$/Ar steam, whereas in the absence of steam, the production of hydrogen decays rapidly due to the accumulation of carbonaceous deposits, in line with the above discussion.

### 3.3. Mechanistic insights

The observed findings enable rationalizing the impact of steam on the reaction pathway proposed for the $Rh/MgAl_2O_4$ catalyst in the absence and presence of water (Fig. 8a and b). Under both reaction conditions, $CO_2$ and $CH_4$ were dissociatively adsorbed over the metal surface. The resulting $CH_x$ species react, either over the metal surface or at the metal support interface, with close active O* atoms, producing $CH_xO$ species, which decompose to CO and $H_2$. Still, remarkable differences concerning the type of surface species developed on the surface and Rh–CO interactions were observed. In our previous work, we found that the dissociative adsorption of $CO_2$ over Rh metal surfaces was associated with the partial oxidation and re-dispersion of Rh atoms.[31] The lower-coordinated Rh cluster were proposed to promote the generation of stable bridged carbonyls through the decomposition of unstable geminal carbonyls. In fact, it is generally accepted that the nature and geometry of the active metal determines the dissociation of $CH_4$ and the overall catalyst performance. Herein, we observed that bridged carbonyl bands were developed over two different Rh

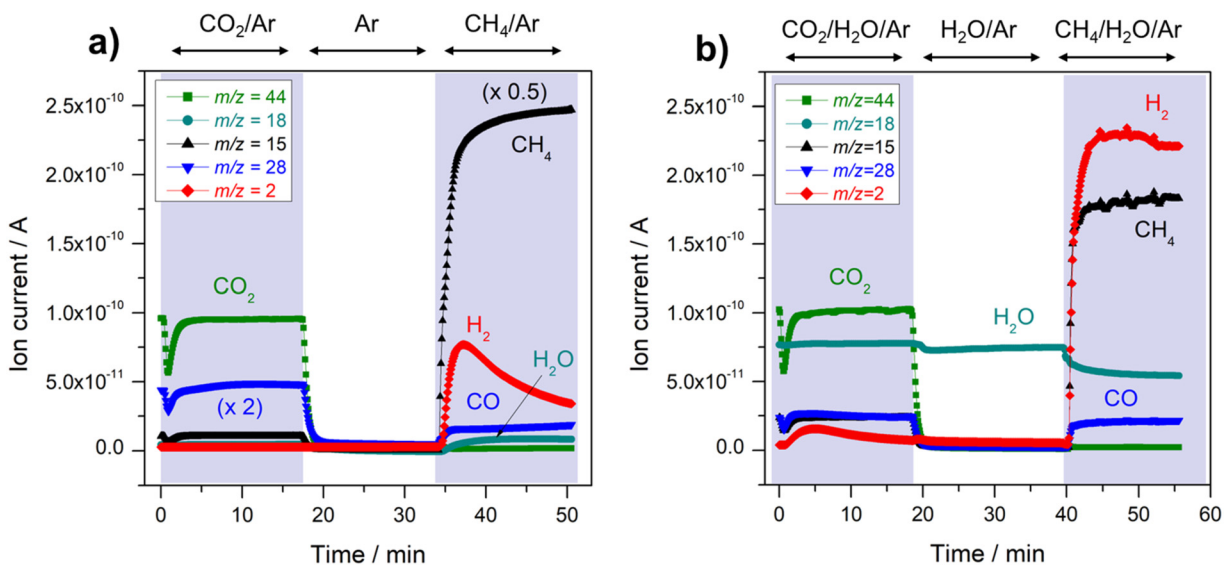


Fig. 7 Evolution of the gas-phase analysed on-line by MS as a function of time-on-stream under the sequential switching of the feed gas in the absence a) and presence of steam b).

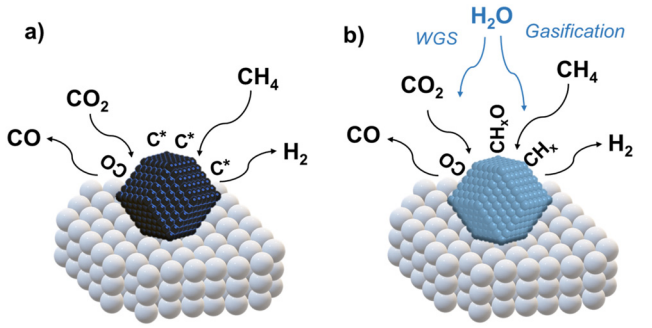


Fig. 8 Proposed reaction pathways in the absence a) and presence of steam b).

surface adsorption sites. In this sense, the disappearance of stable bridged carbonyl might undermine the catalyst performance by blocking the Rh active sites through the generation of carbon species *via* Boudouard's and methane cracking reactions. The catalysts' deactivation derived from the coke deposits generated over the Rh surface in the absence of water agrees with the hydrogen drop observed in the MS analysis at higher temperatures (Fig. 5a).

In the presence of steam, the absence of carbonaceous deposits observed on the catalysts surface and the greater $CH_4$ conversion rates suggest that water molecules facilitate the decomposition of reaction intermediates into $H_2$ and CO. From the *operando* DRIFT-MS results, the hydroxylated surface could improve the reaction of the CO* species with the nearby OH species, generating $CH_xO$ species that subsequently decomposes into the reaction products. Besides, the presence of water should also promote the forward WGS reaction, removing CO species from the metal surface, thereby hindering coke generation *via* the Boudouard reaction. Remarkably, the incorporation of water molecules also constricted the blocking of Rh active sites. In this sense, steam could promote the exposition of Rh surface active for methane decomposition to some extent and inhibit the accumulation of stable carbonaceous species over highly dispersed Rh sites. In all, the incorporation of water molecules enhances the performance of the $Rh/MgAl_2O_4$ catalyst by promoting the generation of $CH_xO$ species, enhancing the decomposition of carbonaceous species and inhibiting the accumulation of carbon deposits over the active Rh metal surfaces.

## 4. Concluding remarks

This work analyses the benefits attained by incorporating water into DRM stream over the $Rh/MgAl_2O_4$ catalyst by combining steady-state and transient *operando* DRIFT coupled with MS spectrometry. The catalytic activity results evidenced the generation of syngas with higher $H_2/CO$ ratios because of the promotion of $CH_4$ conversion and lower $CO_2$ conversions due to the impact of the forward WGS reaction. The incorporation of water affected the constituted Rh nanoparticles and reaction intermediates both in nature and concentration. Hence, the hydroxylated surface attained in the presence of water enhanced the reactivity of $CH_x$ species with the active O* species, thereby enhancing the generation of $CH_xO$ species, the proposed major reaction intermediate towards $H_2$ production. Moreover, the presence of steam promoted the decomposition of carbonaceous species and constricted the coking phenomena over the metal surface, thus enhancing the catalyst lifetime.

## Conflicts of interest

There are no conflicts to declare.

## Acknowledgements

Dra. Miriam González acknowledges to the EMERGIA program of the Junta de Andalucía by the EMC21_00052 contract. The authors acknowledge financial support from Spanish Ministry of Science through the projects NICER-BIOFUELS (PLEC2021-008086) financed by Next Generation European Funds and SMART-FTS (PID2021-126876OB-I00).

## References

1 P. Verma and S. K. Samanta, in *Proceedings of the First International Conference on Recent Advances in Bioenergy Research*, 2016, pp. 227–243.
2 M. González-Castaño, M. H. Kour, J. González-Arias, F. M. Baena-Moreno and H. Arellano-Garcia, *J. Environ. Manage.*, 2021, **300**, 1–8.
3 L. Yang, X. Ge, C. Wan, F. Yu and Y. Li, *Renewable Sustainable Energy Rev.*, 2014, **40**, 1133–1152.
4 M. Tabatabaei, M. Aghbashlo, E. Valijanian, H. Kazemi Shariat Panahi, A.-S. Nizami, H. Ghanavati, A. Sulaiman, S. Mirmohamadsadeghi and K. Karimi, *Renewable Energy*, 2020, **146**, 1392–1407.
5 P. Ferreira-Aparicio, M. J. Benito and J. L. Sanz, *Catal. Rev.: Sci. Eng.*, 2005, **47**, 491–588.
6 S. Rasi, J. Lehtinen and J. Rintala, *Renewable Energy*, 2010, **35**, 2666–2673.
7 M. Gustafsson and N. Svensson, *J. Cleaner Prod.*, 2021, **278**, 123535.
8 P. S. Roy, J. Song, K. Kim, C. S. Park and A. S. K. Raju, *J. CO2 Util.*, 2018, **25**, 275–282.
9 I. Ullah Khan, M. Hafiz Dzarfan Othman, H. Hashim, T. Matsuura, A. F. Ismail, M. Rezaei-DashtArzhandi and I. Wan Azelee, *Energy Convers. Manage.*, 2017, **150**, 277–294.
10 P. Tarifa, T. R. Reina, M. González-Castaño and H. Arellano-García, *Energy Fuels*, 2022, **36**(15), 8267–8273.
11 S. Sarker, J. J. Lamb, D. R. Hjelme and K. M. Lien, *Fuel*, 2018, **226**, 686–697.
12 J. He, N. Han, M. Xia, T. Sun and H. Ghaebi, *Int. J. Hydrogen Energy*, 2023, **48**, 21161–21175.
13 H. Zhang, Z. Sun and Y. H. Hu, *Renewable Sustainable Energy Rev.*, 2021, **149**, 111330.
14 A. M. Álvarez, M. Á. Centeno and J. A. Odriozola, *Top. Catal.*, 2016, **59**, 303–313.

15 N. Kumar, M. Shojaee and J. J. Spivey, *Curr. Opin. Chem. Eng.*, 2015, **9**, 8–15.
16 M. M. Danilova, Z. A. Fedorova, V. A. Kuzmin, V. I. Zaikovskii, A. V. Porsin and T. A. Krieger, *Catal. Sci. Technol.*, 2015, **5**, 2761–2768.
17 L. Kaiwen, Y. Bin and Z. Tao, *Energy Sources, Part B*, 2018, **13**, 109–115.
18 R. Ma, B. Xu and X. Zhang, *Catal. Today*, 2019, **338**, 18–30.
19 K. Jabbour, N. El Hassan, A. Davidson, S. Casale and P. Massiani, *Catal. Sci. Technol.*, 2016, **6**, 4616–4631.
20 S. Arora and R. Prasad, *RSC Adv.*, 2016, **6**, 108668–108688.
21 T. Stroud, T. J. Smith, E. Le Saché, J. L. Santos, M. A. Centeno, H. Arellano-Garcia, J. A. Odriozola and T. R. Reina, *Appl. Catal., B*, 2018, **224**, 125–135.
22 Z. Zhao, P. Ren, W. Li and B. Miao, *Int. J. Hydrogen Energy*, 2016, 1–12.
23 Z. Geng, J. Gao, H. Dong and S. Wang, *React. Kinet., Mech. Catal.*, 2022, **135**, 705–721.
24 W. J. Jang, D. W. Jeong, J. O. Shim, H. M. Kim, H. S. Roh, I. H. Son and S. J. Lee, *Appl. Energy*, 2016, **173**, 80–91.
25 B. A. V. Santos, J. M. Loureiro, A. M. Ribeiro, A. E. Rodrigues and A. F. Cunha, *Can. J. Chem. Eng.*, 2015, **93**, 510–526.
26 F. B. Noronha, M. C. Durão, M. S. Batista and L. G. Appel, *Catal. Today*, 2003, **85**, 13–21.
27 A. Brush, E. J. Evans, G. M. Mullen, K. Jarvis and C. B. Mullins, *Fuel Process. Technol.*, 2016, **153**, 111–120.
28 V. A. Kondratenko, U. Karimova, A. A. Kasimov and E. V. Kondratenko, *Appl. Catal., A*, 2021, **619**, 118143.
29 M. Maestri, D. G. Vlachos, A. Beretta, G. Groppi and E. Tronconi, *J. Catal.*, 2008, **259**, 211–222.
30 J. R. Rostrup-Nielsen and J. H. Bak Hansen, *J. Catal.*, 1993, **144**, 38–49.
31 L. F. Bobadilla, V. Garcilaso, M. A. Centeno and J. A. Odriozola, *ChemSusChem*, 2017, **10**, 1193–1201.
32 K. Jabbour, *J. Energy Chem.*, 2020, **48**, 54–91.
33 S. Yu, Y. Hu, H. Cui, Z. Cheng and Z. Zhou, *Chem. Eng. Sci.*, 2021, **232**, 116379.
34 M. Alabdullah, M. Ibrahim, D. Dhawale, J. A. Bau, A. Harale, S. Katikaneni and J. Gascon, *ChemCatChem*, 2021, **13**, 2879–2886.
35 S. Singh, M. B. Bahari, B. Abdullah, P. T. T. Phuong, Q. D. Truong, D. V. N. Vo and A. A. Adesina, *Int. J. Hydrogen Energy*, 2018, **43**, 17230–17243.
36 K.-J. Kim, K. Y. Kim, G. B. Rhim, M. H. Youn, Y.-L. Lee, D. H. Chun and H.-S. Roh, *Chem. Eng. J.*, 2023, **468**, 143632.
37 C. Morterra, C. Emanuel, G. Cerrato and G. Magnacca, *J. Chem. Soc., Faraday Trans.*, 1992, **88**, 339–348.
38 F. Romero-Sarria, S. Garcia-Dali, S. Palma, E. M. Jimenez-Barrera, L. Oliviero, P. Bazin and J. A. Odriozola, *Surf. Sci.*, 2016, **648**, 84–91.
39 C. Morterra, G. Ghiotti, F. Boccuzi and S. Coluccia, *J. Catal.*, 1978, **51**, 299–313.
40 E. Finocchio, G. Busca, P. Forzatti, G. Groppi and A. Beretta, *Langmuir*, 2007, **23**, 10419–10428.
41 R. Büchel, A. Baiker and S. E. Pratsinis, *Appl. Catal., A*, 2014, **477**, 93–101.
42 A. Beuls, C. Swalus, M. Jacquemin, G. Heyen, A. Karelovic and P. Ruiz, *Appl. Catal., B*, 2012, **113–114**, 2–10.
43 F. Azzolina-Jury and F. Thibault-Starzyk, *Top. Catal.*, 2017, **60**, 1709–1721.
44 Z. Ferencz, K. Baán, A. Oszkó, Z. Kónya, T. Kecskés and A. Erdohelyi, *Catal. Today*, 2014, **228**, 123–130.
45 R. Castillo, E. Dominguez Garcia, J. L. Santos, M. A. Centeno, F. Romero Sarria, M. Daturi and J. A. Odriozola, *Catal. Today*, 2020, **356**, 390–398.
46 J. I. Di Cosimo, V. K. Díez, M. Xu, E. Iglesia and C. R. Apesteguía, *J. Catal.*, 1998, **178**, 499–510.
47 G. Busca and V. Lorenzelli, *Mater. Chem.*, 1982, **7**, 89–126.
48 D. Lorito, P. Fongarland and Y. Schuurman, *Ind. Eng. Chem. Res.*, 2021, **60**, 6698–6705.
49 K. Hadjiivanov, J.-C. Lavalley, J. Lamotte, F. Maugé, J. Saint-Just and M. Che, *J. Catal.*, 1998, **176**, 415–425.
50 E. Jiménez-Barrera, P. Bazin, C. Lopez-Cartes, F. Romero-Sarria, M. Daturi and J. A. Odriozola, *Appl. Catal., B*, 2018, **237**, 986–995.
51 F. Solymosi, *J. Catal.*, 1982, **75**, 78–93.
52 P. B. Rasband and W. C. Hecker, *J. Catal.*, 1993, **139**, 551–560.
53 J. C. Lavalley, J. Saussey, J. Lamotte, R. Breault, J. P. Hindermann and A. Kiennemann, *J. Phys. Chem.*, 1990, **94**, 5941–5947.
54 B. Wang, L. Song and R. Zhang, *Appl. Surf. Sci.*, 2012, **258**, 3714–3722.
55 A. M. Hernández-Giménez, J. Ruiz-Martínez, B. Puértolas, J. Pérez-Ramírez, P. C. A. Bruijnincx and B. M. Weckhuysen, *Top. Catal.*, 2017, **60**, 1522–1536.
56 F. Romero-Sarria, L. F. Bobadilla, E. M. Jiménez Barrera and J. A. Odriozola, *Appl. Catal., B*, 2020, **272**, 119032.
57 L. Azancot, L. F. Bobadilla, M. A. Centeno and J. A. Odriozola, *Fuel*, 2022, **320**, 123843.
58 Q. Qian, J. Ruiz-Martínez, M. Mokhtar, A. M. Asiri, S. A. Al-Thabaiti, S. N. Basahel, H. E. van der Bij, J. Kornatowski and B. M. Weckhuysen, *Chem. – Eur. J.*, 2013, **19**, 11204–11215.
59 Q. Qian, J. Ruiz-Martínez, M. Mokhtar, A. M. Asiri, S. A. Al-Thabaiti, S. N. Basahel and B. M. Weckhuysen, *Catal. Today*, 2014, **226**, 14–24.